Supporting Information

(9 pages, including 9 Figures and 1 Table)

CVD Carbon-Coated Carbonized Loofah Sponge Loaded with Directionally Arrayed MXene Aerogel for Electromagnetic Interference Shielding

Songtao Li,[ab] Jiashun Wang,[ab] Zhengwang Zhu,[ab] Dongyan Liu,[ab] Wanchong Li,*[a] Guoxin Sui*[ab] and Chul B. Park*[c]

[a] Shi-changxu Innovation Center for Advanced Materials, Institute of Metal Research, Chinese Academy of Sciences, No. 72 Wenhua Road, Shenhe District, Shenyang 110016, China

[b] School of Materials Science and Engineering, University of Science and Technology of China, No. 72 Wenhua Road, Shenhe District, Shenyang 110016, China

[c] Microcellular Plastics Manufacturing Laboratory, Department of Mechanical and Industrial Engineering, University of Toronto, Toronto, Ontario M5S 3G8, Canada

Corresponding Author

*W.C.L.: e-mail, liwanchong@imr.ac.cn.

*G.X.S.: e-mail, gxsui@imr.ac.cn; Tel, +86 24 83978040.

*C.B.P.: e-mail, park@mie.utoronto.ca; Tel, +1 416 978 3053.

CONTENT

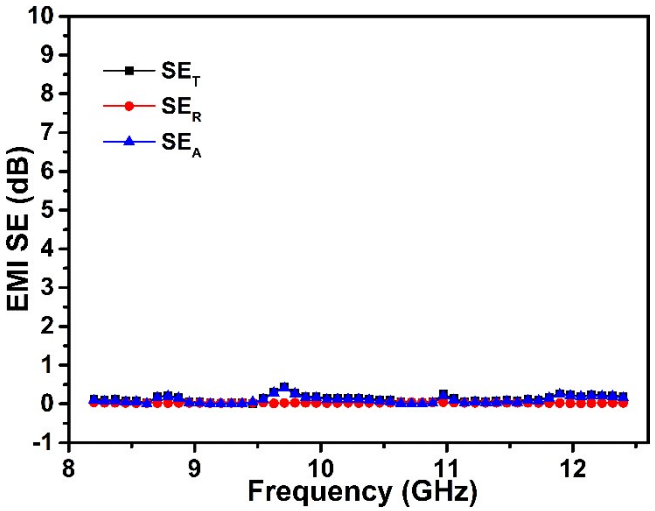

Figure S1. The SE_T, SE_A, and SE_R of pure loofah sponge (thickness:3.2 mm) in the frequency range of 8.2–12.4 GHz

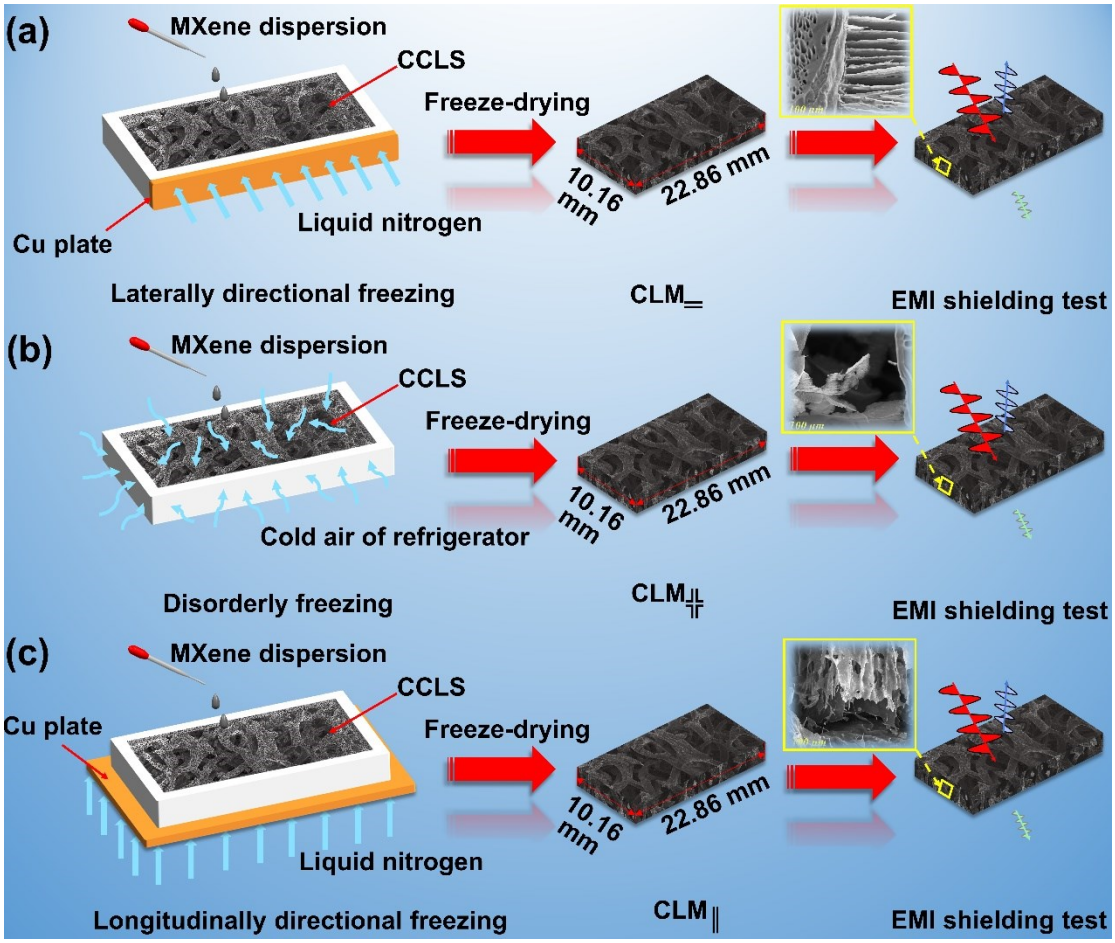

Figure S2. Schematic illustration of preparation and EMI shielding test process of CCLS-60/MXene aerogel composites

Theoretical explanation of shielding effectiveness

The electromagnetic shielding effectiveness of the composite material is theoretically calculated based on the electromagnetic parameters (S). The S parameters correspond to the reflected (S_{11} or S_{22}) and transmitted (S_{21} or S_{12}) powers. Full two-port Thru-Reflect-Line (TRL) calibration was initially performed on the VNA. The shielding effectiveness is defined as the logarithm of the ratio of the incident power (P_i) to the transmitted power (P_0), and the total shielding effectiveness (SE_T) consists of reflection (SE_R), absorption (SE_A) and multiple reflections (SE_M) according to the transmission line model theory, the relationship is as follows

$$SE_T(dB) = 10\lg\left(\frac{P_i}{P_0}\right) = SE_R + SE_A + SE_M \quad \text{(S1)}$$

With higher EMI SE values and absorption dominated, the SE_M may be ignored. Additionally, the SE_R and SE_A are related to the coefficients of reflection (R), absorption (A) and transmission (T) that can be calculated from S parameters, the formula is as follows[1]

$$SE_R(dB) = 10\lg\left(\frac{1}{1-R}\right) \quad \text{(S2)}$$

$$SE_A(dB) = 10\lg\left(\frac{1-R}{T}\right) \quad \text{(S3)}$$

$$1 = R + A + T \quad \text{(S4)}$$

$$R = |S_{11}|^2 = |S_{22}|^2, T = |S_{21}|^2 = |S_{12}|^2 \quad \text{(S5)}$$

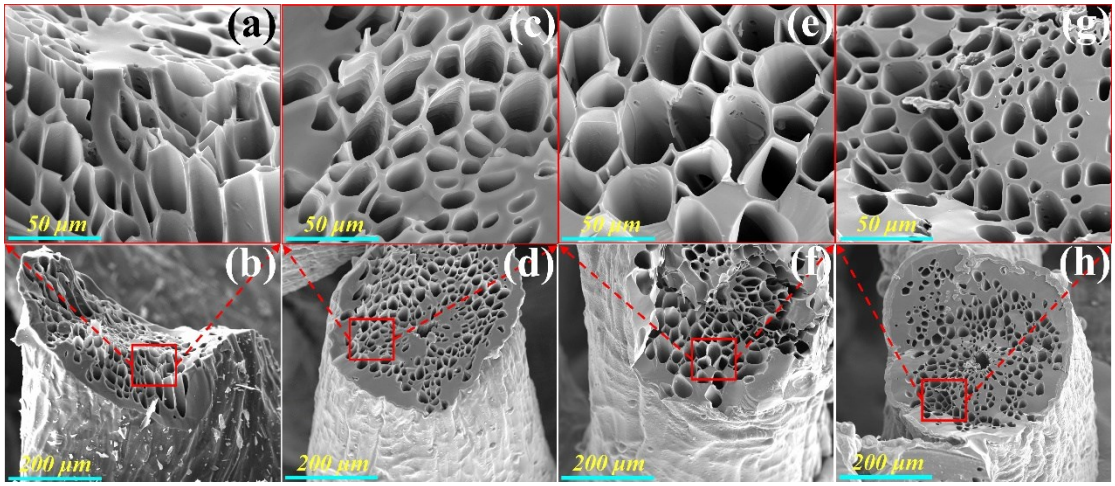

Figure S3. (a-b) SEM images of the fiber cross-section of CPLS, (c-d) CCLS-16, (e-f) CCLS-40, and (g-h) CCLS-60

Figure S4 shows the characteristic peaks of Raman spectrum of MXene ($Ti_3C_2T_x$) at around 201, 392, 571, 626, and 724 cm^{-1}. The peak Ⅰ disappears, while peak Ⅱ broadens and down shift, suggesting the loss of Al element and the exfoliation of MAX phase.[2]

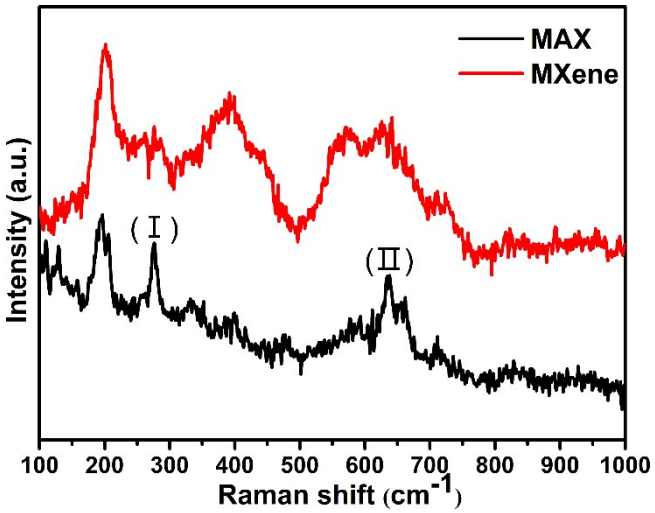

Figure S4. Raman spectra of MAX (Ti_3AlC_2) phase and MXene ($Ti_3C_2T_x$)

In order to further investigate the EMI shielding mechanisms of CLM composites, the reflection (R), absorption (A), and transmission (T) coefficients of CLM10₋,

CLM15═, and CLM20═ were calculated and analyzed by the measured S parameters. It can be seen from **Figure S5** that the R values gradually increase with the enhancement on concentration of MXene dispersion, while the T and A values decrease, indicating the reflecting microwave ability increases and the absorbing microwave ability decreases for the CLM composites. The reason may be due to the increase in electrical conductivity of composites, resulting in an enhancement in the degree of interface mismatch. Although the R values increase and the A values decrease, the interaction interfaces of CLM composites that attenuate incident microwave continually increase. In theory, the attenuation of incident microwave is closely related to the interaction interfaces of shielding materials. The more interaction interfaces, the stronger interface polarization. Consequently, the contribution of shielding absorption is greater than that of shielding reflection for the EMI shielding performance of CLM composites.

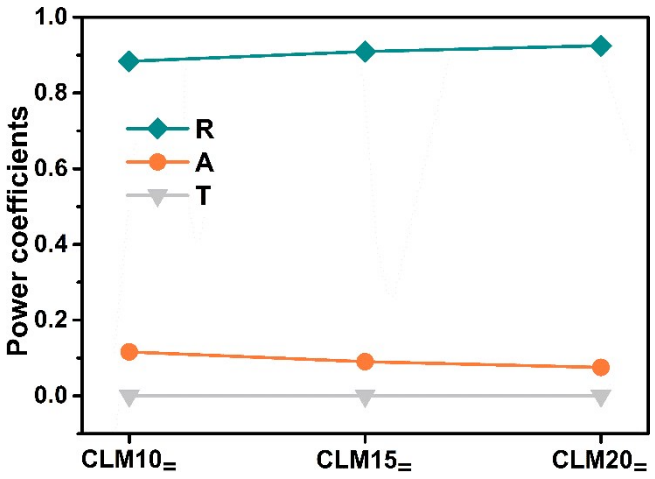

Figure S5. (a) Average A, T, and R values of the CLM with different MXene concentrations in the frequency range of 8.2–12.4 GHz

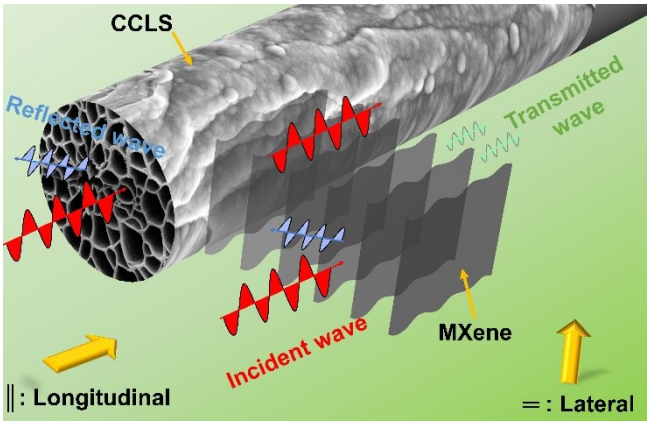

Figure S6. Schematic diagram of electromagnetic shielding mechanism analysis of $CLM_{\parallel}$ composites

Figure S7 depicts the comparison of XRD patterns for CLM20═ and burnt CLM20═. Obviously, the XRD curve of burnt CLM20═ shows that the diffraction peaks located at 25.32° and 27.38° correspond to the (101) plane of anatase TiO_2 and the (110) plane of rutile TiO_2, respectively.[3] This fully explains the MXene in the CLM20═ composite is oxidized after being burnt by the flame of the alcohol burner.

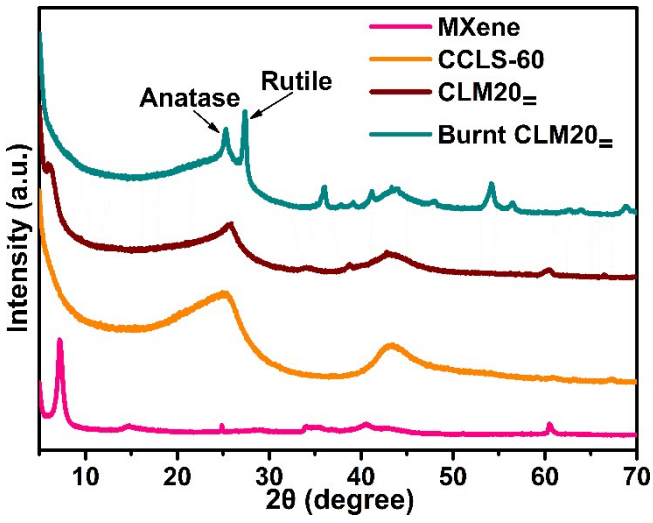

Figure S7. XRD patterns of MXene, CCLS-60, CLM20═, and burnt CLM20═

Table S1. Thermal property of the CPLS and CCLS

Sample designation	T_5 (°C)	T_{10} (°C)	T_{max} (°C)
CPLS	384.2	403.2	432.0
CCLS-16	570.5	597.7	666.5
CCLS-40	597.8	614.8	704.9
CCLS-60	615.5	634.7	800.8

T_5 = Temperature of 5% weight loss;

T_{10} = Temperature of 10% weight loss;

T_{max} = Maximum decomposition temperature.

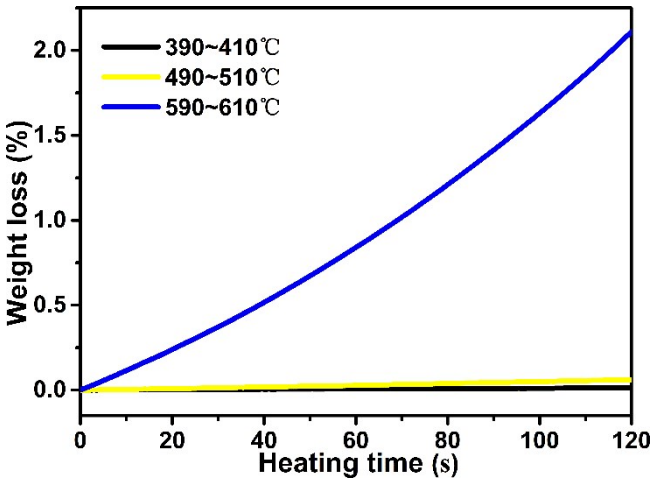

Figure S8. The weight loss curve of CCLS-60 as a function of heating time in different temperature ranges

There is no clear damage and crack in the surface of CCLS-60 after the CLM20═ is burnt for 120 s (**Figure S9)**. In contrast, the MXene aerogel undergoes severe damage due to pyrolysis shrinkage. Furthermore, the MXene is transformed to TiO_2 due to the oxidation reaction. When the CLM20═ is burnt, the great flame resistance of MXene endows it a protective effect to block out a part of fire for the CCLS-60.

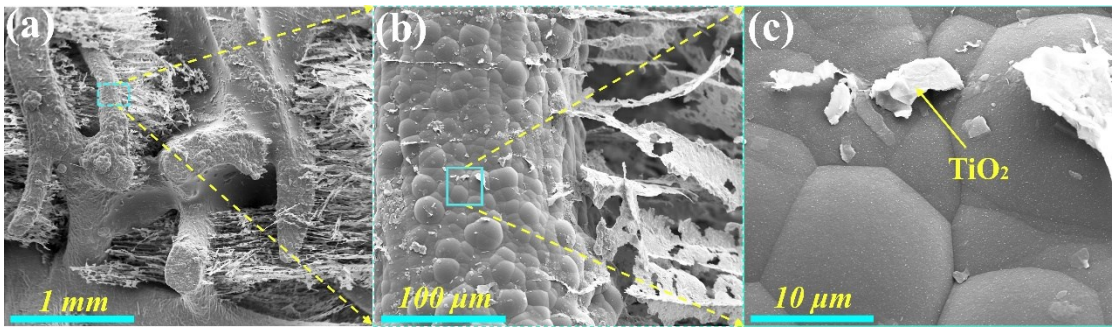

Figure S9. SEM images of CLM20₌ after being burnt for 120 s

REFERENCES

1 F. Shahzad, M. Alhabeb, C. B. Hatter, B. Anasori, S. M. Hong, C. M. Koo, Y. Gogotsi, *Science*, 2016, 353, 1137-1140.

2 X. Li, X. Yin, S. Liang, M. Li, L. Cheng, L. Zhang, Carbon 2019, 146, 210-217.

3 L. Li, Y. Cao, X. Liu, J. Wang, Y. Yang, W. Wang, *ACS Appl. Mater. Interfaces*, 2020, *12* (24), 27350-27360.